Neuronal and epithelial cell rescue resolves chronic systemic inflammation in the lipid storage disorder Niemann-Pick C

Manuel E. Lopez[1,2], Andrés D. Klein[1,2], Jennifer Hong[1,2], Ubah J. Dimbil[1,2] and Matthew P. Scott[1,2,*]

[1]Department of Developmental Biology and [2]Department of Genetics, and Bioengineering, Howard Hughes Medical Institute, Stanford University School of Medicine Clark Center, 318 Campus Drive, Stanford, CA 94305-5439, USA

Chronic systemic inflammation is thought to be a major contributor to metabolic and neurodegenerative diseases. Since inflammatory components are shared among different disorders, targeting inflammation is an attractive option for mitigating disease. To test the significance of inflammation in the lipid storage disorder (LSD) Niemann-Pick C (NPC), we deleted the macrophage inflammatory gene *Mip1a/Ccl3* from NPC diseased mice. Deletion of *Ccl3* had been reported to delay neuronal loss in Sandhoff LSD mice by inhibiting macrophage infiltration. For NPC mice, in contrast, deleting *Ccl3* did not retard neurodegeneration and worsened the clinical outcome. Depletion of visceral tissue macrophages also did not alter central nervous system (CNS) pathology and instead increased liver injury, suggesting a limited macrophage infiltration response into the CNS and a beneficial role of macrophage activity in visceral tissue. Prevention of neuron loss or liver injury, even at late stages in the disease, was achieved through specific rescue of NPC disease in neurons or in liver epithelial cells, respectively. Local epithelial cell correction was also sufficient to reduce the macrophage-associated pathology in lung tissue. These results demonstrate that elevated inflammation and macrophage activity does not necessarily contribute to neurodegeneration and tissue injury, and LSD defects in immune cells may not preclude an appropriate inflammatory response. We conclude that inflammation remains secondary to neuronal and epithelial cell dysfunction and does not irreversibly contribute to the pathogenic cascade in NPC disease. Without further exploration of possible beneficial roles of inflammatory mediators, targeting inflammation may not be therapeutically effective at ameliorating disease severity.

INTRODUCTION

The continuous elevation of inflammatory cytokines, lysosomal defects in microglia and macrophages, and other immune system irregularities have been proposed to play important roles in promoting tissue damage and neurodegeneration in lipid storage disorders (LSDs) (1–6). If the inflammatory process is harmful, therapeutically targeting immune cells and inflammatory mediators may provide a way to mitigate disease progression for these devastating and as yet incurable diseases. Here, we explore the role of inflammation in the severity and progression of the neurodegenerative lysosomal storage disease Niemann-Pick C (NPC).

NPC is a rare complex metabolic LSD that leads to progressive deterioration of the nervous system and multiple organ systems in the body (7). Although rare, NPC shares many molecular and pathological mechanisms with more common unrelated disorders. Patients with NPC have changes in brain biomarkers that are associated with Alzheimer's disease (8) and suffer multiple neurological symptoms, such as dementia, dystonia, seizures and psychiatric disorders. NPC also exhibits a number of immune cell phenotypes. Macrophage foam cells

---

*To whom correspondence should be addressed at: Stanford University, Clark Center W200, 318 Campus Drive, Stanford, CA 94305, USA. Tel: +1 6507257656; Fax: +1 6507252952; Email: mscott@stanford.edu

are a common pathological occurrence in NPC (9) and are well known for their role in atherosclerosis, where they form plaques in the circulatory system (10). Mouse studies of NPC have shown impaired natural killer T cell development (11), as well as abnormal production of complement components that are involved in the neuroinflammatory process of many neurodegenerative diseases (12). Knowledge obtained from studying NPC pathology will likely aid in understanding pathological processes of other LSDs and of neurodegenerative diseases with similar pathologies.

NPC disease is caused by genetic loss of *NPC1* function resulting in defective intracellular lipid flux and accumulation of lysosomal material that is potentially deleterious to cells. NPC1 is a 13-pass endosomal/lysosomal membrane protein that binds cholesterol, and more strongly oxysterols, *in vitro* (13,14). While most cases of NPC disease are caused by *NPC1* gene mutations, *NPC2* loss of function causes a nearly identical disease. Unlike NPC1, NPC2 is a soluble secreted sterol-binding protein that can be found in the lumens of endosomes and lysosomes (15). It has been hypothesized that both proteins shuttle cholesterol between each other and endosomal/lysosomal membranes to facilitate the exit of free cholesterol from the lysosome (16,17). A defect in this process alters intracellular lipid homeostasis, membrane properties and proper intracellular trafficking of organelles (18–20). The consequent accumulation of lysosomal material, e.g. sterols, gangliosides and sphingolipids, is seen in virtually every cell in the body.

Despite a ubiquitous storage defect, only certain cell types, such as neurons and hepatocytes, are particularly susceptible to dysfunction and injury. Both NPC proteins are also essential for proper macrophage and lymphocyte maturation and function (11,21–23), but whether defects in immune cells relate to the pathogenesis of NPC disease is unclear. It is reasonable to believe that aberrant or excessive inflammatory responses elicited by NPC defects may contribute to disease pathology and progression.

Although the genetic causes of NPC are well understood, how best to mitigate disease pathology remains unknown. We set out to determine to what extent immune cell activity influences NPC disease progression. Investigations into NPC disease biology are facilitated by naturally occurring mammalian models that recapitulate the human condition (24,25). In our effort to control inflammation and correct NPC disease pathology, we pursued various complementary approaches using the $Npc1^{-/-}$ mouse model of the disease, also known as npc^{nih} (24).

To determine the contribution of macrophage and microglial-mediated inflammation to the severity of NPC disease, we genetically deleted the macrophage inflammatory protein 1alpha gene, *Mip1a*/*Ccl3*. CCL3 protein is a known pro-inflammatory cytokine that can mediate chemotaxis of monocytes and promote cell degranulation (26). *Ccl3* expression is elevated in the central nervous system (CNS) and visceral tissue of many LSDs, including Sandhoff disease, a prototypical autoimmune-like LSD (27–32). The deletion of *Ccl3* in a mouse model of Sandhoff disease resulted in reduced monocyte-associated pathology in the brain, delayed neurodegeneration and prolonged health (31). Sandhoff and NPC should share common pathological mechanisms, since both disorders cause ganglioside storage defects and immune cell impairment (33). If the NPC

pathogenic cascade behaves the same as in Sandhoff disease, deletion of *Ccl3* should be beneficial to $Npc1^{-/-}$ mice.

In a second approach, we determine whether the inflammatory response and disease pathology is refractory to restoration of NPC1 function after tissue damage has been established. The findings obtained are critically important with respect to determining the timing of treatments and in elucidating what cell types are necessary to target to halt disease progression and elicit recovery. Previously, it was postulated that the failure of current treatments such as cyclodextrin (CYCLO) to correct the pathology of tissues such as the lung was due to the inability of CYCLO to reach lung macrophages (27,34). This reasoning assumed that the activities of macrophages, driven by their own NPC storage defects, continuously promote cell death and tissue injury in LSDs. To address these issues, we used an established cell-specific transgene form of gene therapy to genetically manipulate the production of NPC1 with cell and tissue specificity in otherwise $Npc1^{-/-}$ mice. In the past, we exploited the cell-autonomous nature of $Npc1^{-/-}$ defects in mice to show that neuron-specific rescue, but not astrocyte-specific rescue, prevented or delayed neurological disease signs (35). In this report, we used features of the engineered mice that allowed control of *timing* of NPC rescue. This temporal and cell-type-specific rescue system allowed us to assess the importance of correcting the NPC defect in $Npc1^{-/-}$ macrophages and microglia by determining whether restoring NPC1 function only in neurons and epithelial cells, even late in the disease, would be sufficient to halt cell injury and lessen the inflammatory response.

Together, our studies demonstrate that inflammatory mediators such as cytokines and macrophages have distinct disease relevance even in LSDs with similar storage defects. Perturbing part of the inflammatory pathway did not improve the health of mice with NPC disease even though the same procedure was successful for mice with Sandhoff disease. We propose that the role of inflammation in NPC disease is potentially beneficial and should be mainly viewed as a reaction to local neuron and epithelial cell defects since disease pathology can be halted or reversed by rescuing these cell types. Our conclusions highlight the importance of determining the contribution of each cell type to the clinical state of a particular storage disorder in order to better justify whether or not to pursue certain therapeutic avenues. The findings also have implications for further classifying LSDs according to whether macrophage activity and inflammatory mediators cause or exacerbate cell injury.

RESULTS

Elevated regional *Ccl3* expression in NPC-diseased mice

Elevated expression of genes encoding pro-inflammatory mediators has been previously observed in brains of $Npc1^{-/-}$ mice at 21 days of age, and correlates well with increased glial-mediated inflammation (12). Here, we show that at 50 days of age, preceding a notable decline in mouse weight that indicates deteriorating health, the expression of *Ccl3* was ranked using microarrays as one of the most elevated inflammatory mediators in $Npc1^{-/-}$ mouse cerebella (Fig. 1A). Significance analysis of microarrays (SAM) (36), with the incorporation of
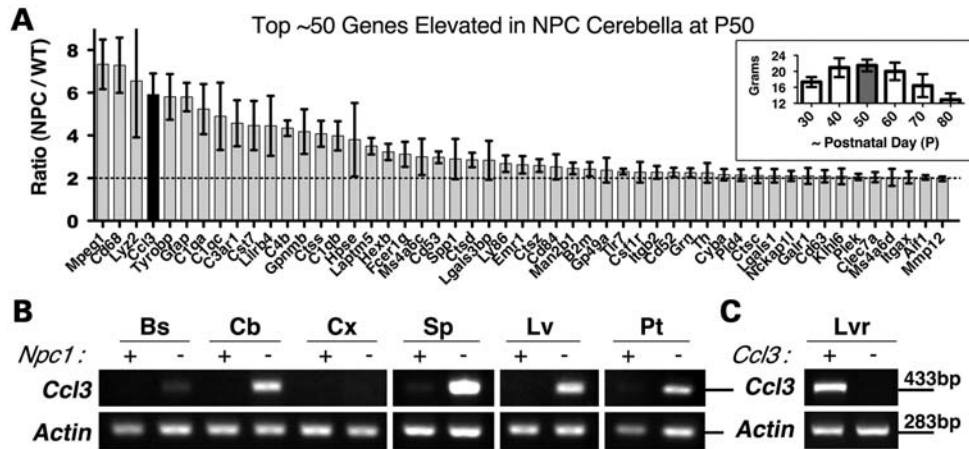
Figure 1. *Ccl3* gene expression is elevated in the brain and visceral tissues of NPC mice. (**A**) We carried out gene expression profile analyses of *Npc1*$^{-/-}$ mice (NPC) compared with *Npc1*$^{+/-}$ mice (WT) cerebella at P50, an age before weight loss is detected in *Npc1*$^{-/-}$ mice (boxed inset, $n = 12$). *Ccl3* (black bar) was among the most elevated mRNAs identified. Representative data from microarrays of cerebella from two age-matched *Npc1*$^{-/-}$ mice and three age-matched *Npc1*$^{+/-}$ mice are shown. (**B**) Reverse transcription (RT)–polymerase chain reaction (PCR) analysis performed on *Npc1*$^{-/-}$ (*Npc1*−) mice at age P60 revealed region-specific elevation of *Ccl3* mRNA in the brain compared with *Npc1*$^{+/-}$ (*Npc1* +) mice. Highest expression was detected in the cerebellum (Cb), less in brainstem (Bs) and lowest in the cortex (Cx). Elevated levels of *Ccl3* mRNA were also detected in spleen (Sp), liver (Lv) and isolated peritoneal cells (Pt). (**C**) Control RT–PCR showed the absence of a PCR product derived from *Ccl3*$^{-/-}$ (*Ccl3*−) mouse liver samples. Actin was used to control for RT–PCR conditions and representative data from RT–PCR on samples obtained from three mice are shown (B and C).

array data from age P71 mice, further identified the increase in *Ccl3* expression as significant (q-value = 0) and among the top 18 significantly elevated genes listed, with a false discovery rate of 5.18% (Supplementary Material, Fig. S1). In addition to *Ccl3*, there is elevated expression of complement pathway components, other immune factors, proteases and lysosomal-related protein genes at P50. Many of these genes are common markers of inflammation and their expression is increased in other LSDs and in neurodegenerative diseases, e.g. the LSDs Sandhoff (37) and Gaucher (38), and Alzheimers (39).

Cytokine *Ccl3* mRNA was elevated in *Npc1*$^{-/-}$ mice compared with *Npc1*$^{+/-}$ mice in regions of the brain that have the earliest and greatest signs of neurodegeneration and microglial activity (Fig. 1B). The cerebellum and thalamus are the most visibly affected brain structures and have the earliest onset of neuronal loss (35). The brainstem shows a gradual increase in neuroinflammation at later ages. The cortex does not have microglia invasion as early or severe as in other brain areas, even though considerable lipid accumulation is apparent in neurons there (35). *Ccl3* levels remain low in these regions (Fig. 1B). In the viscera, elevated *Ccl3* mRNA levels can be readily detected in various tissues from *Npc1*$^{-/-}$ mice, including the liver, an organ commonly affected by NPC disease.

To identify the major producers of *Ccl3* in the body, we examined isolated peritoneal cells, which are primarily macrophages and a few lymphocyte types (40). We also examined tissue from spleen, the predominant storage center for macrophages as well as a minor hematopoietic organ in adult mice (41). Levels of *Ccl3* mRNA were elevated in peritoneal cells and spleen from *Npc1*$^{-/-}$ mice compared with *Npc1*$^{+/-}$ mice (Fig. 1B). Based on these expression profiles, it is likely that the CCL3 protein is mainly produced by microglia and macrophages in the brain and visceral tissue of *Npc1*$^{-/-}$ mice, as expected (27,38,42).

Based on the observation that regions of increased *Ccl3* expression correspond to areas of severe brain pathology, we

next asked whether *Ccl3* and the inflammatory process mediated by microglia and macrophage is important to NPC pathology. Data from the *Ccl3* gene deletion study using the *Hexb*$^{-/-}$ mouse model of Sandhoff disease suggested that CCL3 would likewise be a contributing factor in NPC disease. Alternatively, CCL3 may have a neutral or beneficial role in the disease pathology.

Deletion of Ccl3 worsens the NPC disease outcome in mice

To determine whether CCL3 is required for disease progression in *Npc1*$^{-/-}$ mice, we crossed the same *Ccl3*$^{-/-}$ mouse strain (43) previously used in the Sandhoff study to *Npc1*$^{-/-}$ mice. As a standard for neuron rescue, we measured weights of P60 male mice that were *Npc1*$^{-/-}$ but carried a transgene that rescued Purkinje neurons specifically (Fig. 2A). These mice were generated, as detailed in a prior study (35), by mating an *Npc1*$^{+/-}$ mouse homozygous for a Tet-inducible *Npc1* transgene, *tetO-Npc1-YFP (N),* with a *Npc1*$^{+/-}$ mouse homozygous for the cerebellar Purkinje neuron-specific driver *Pcp2-tTA (P)*. The resulting *P; N; Npc1*$^{-/-}$ offspring produced NPC1-YFP protein in cerebellar Purkinje neurons in an otherwise NPC1-deficient animal. This Purkinje neuron-specific correction of NPC disorder elicited temporary but significant health benefits, such as weight gain, relative to non-Purkinje rescued *Npc1*$^{-/-}$ mice. In contrast to Purkinje neuron-rescued mice, male *Npc1*$^{-/-}$ mice carrying the *Ccl3* deletion did not show any improvements in weight (Fig. 2B). *Ccl3*$^{-/-}$; *Npc1*$^{-/-}$ mice instead were more likely to exhibit lower weight profiles than *Npc1*$^{-/-}$ mice and had to be euthanized at ages earlier than P70 (Fig. 2D).

A trend towards early death was also noticed for female mice (data not shown), although differences in weight were less obvious, possibly because young female mice do not exhibit as much weight gain as young males. At around age P60, the average weight difference between female *Npc1*$^{-/-}$
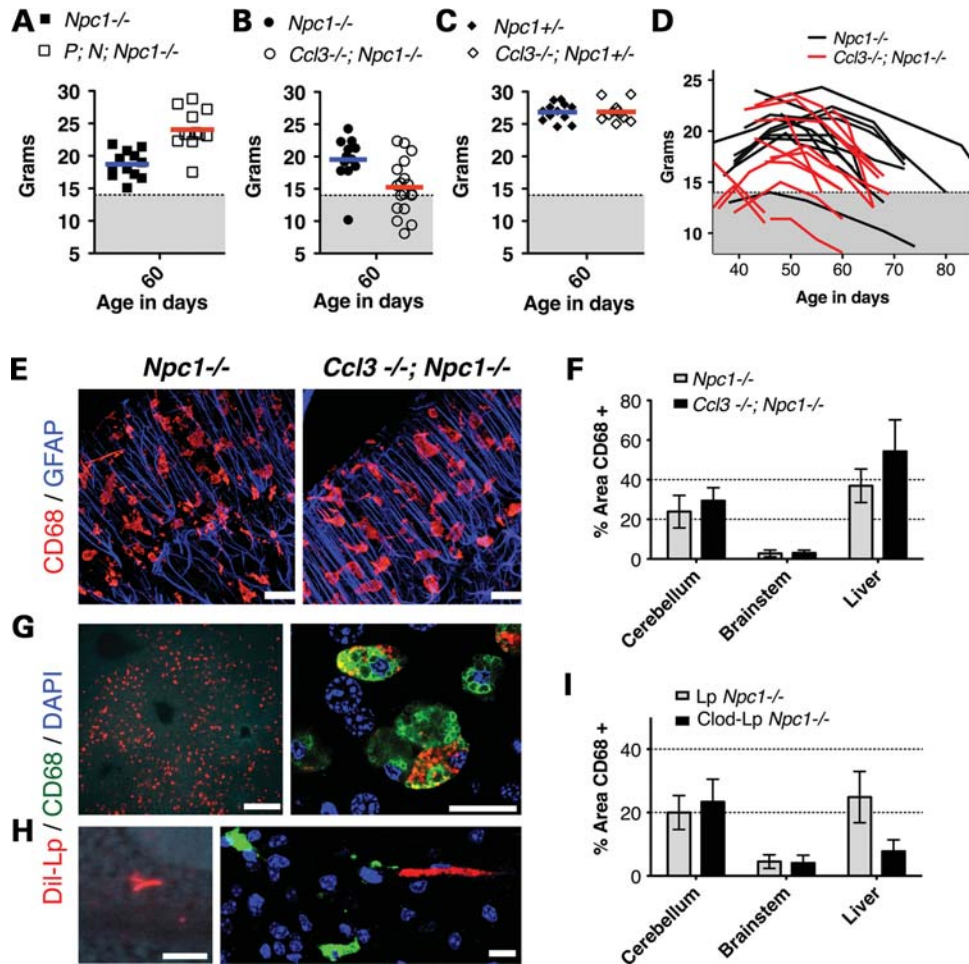
Figure 2. *Ccl3* deletion worsens weight progression and macrophage-associated pathology in NPC mice. (**A**) The individual and average (color line) weight values of diseased mice with rescued cerebellar Purkinje neurons (*P; N; Npc1$^{-/-}$*) were greater than *Npc1$^{-/-}$* mice at age ~P60. *P; N; Npc1$^{-/-}$* and *Npc1$^{-/-}$* mice were in a FVB background. (**B**) In contrast, individual *Ccl3$^{-/-}$; Npc1$^{-/-}$* FVB/B6 mice weights were, on average, lower than *Npc1$^{-/-}$* FVB/B6 mice. A few *Ccl3$^{-/-}$; Npc1$^{-/-}$* mice weights dipped past a predetermined cut-off weight for determining morbidity (dotted horizontal line above gray zone). (**C**) The lack of difference in the average weight of *Ccl3$^{-/-}$; Npc1$^{+/-}$* mice to *Npc1$^{+/-}$* mice at age ~P60 suggested a limited effect of the *Ccl3* gene deletion in non-diseased animals. (**D**) Representative weight curves of 13 *Ccl3$^{-/-}$; Npc1$^{-/-}$* mice (red lines) and 11 *Npc1$^{-/-}$* mice (black lines) are shown. (A–D) Data from male mice are shown. (**E**) CD68 immunofluorescence (red) depicts the differences in microglia/macrophage response in age-matched cerebella at P65. Representative pathology from five mice is shown. Glial fibrillary acidic protein (GFAP) immunofluorescence (blue) depicts Bergmann-glia and astrocytes in the cerebellum. Scale bar is 20 μm. (**F**) Percent areas of tissues that are CD68 positive in the cerebellum and liver were calculated for five *Ccl3$^{-/-}$; Npc1$^{-/-}$* mice. (**G**) After injection of Dil-Lp (red) into the peritoneal cavity of *Npc1$^{-/-}$* mice, which are *Ccl3$^{+/+}$*, the dye was taken up by macrophages (green) in the liver. Scale bars: left panel 200 μm; right panel 20 μm. (**H**) Dil-Lp (red) was not taken up by microglia in the brain (green) and remained in capillaries, identified by morphology. Scale bars: left panel 100 μm; right panel 10 μm. (**I**) Percent areas of tissues that were CD68 positive were calculated for three *Npc1$^{-/-}$* mice that received Clod-Lp peritoneal injections and three age-matched *Npc1$^{-/-}$* mice that received control Lp injections. Depletion of CD68 occurred in the liver but not in the cerebellum.

mice ($n = 24$) and *Ccl3$^{-/-}$; Npc1$^{-/-}$* mice ($n = 13$) was not as striking ($P = 0.3237$, *t*-test) as the difference between male *Npc1$^{-/-}$* mice ($n = 12$) and *Ccl3$^{-/-}$; Npc1$^{-/-}$* mice ($n = 18$) (Fig. 2B; $P = 0.0076$, *t*-test). Two-way analysis of variance performed on a cohort of nine male and five female pairs further verified that between the ages of 45 and 60, weight curves of female *Npc1$^{-/-}$* and *Ccl3$^{-/-}$; Npc1$^{-/-}$* mice were not significantly different ($P = 0.2028$), but weight curves of male mice were ($P = 0.0045$).

The lower weight phenotype and earlier deaths of *Ccl3$^{-/-}$; Npc1$^{-/-}$* mice was unexpected. This worsening disease profile may be due to an inherent deleterious effect of *Ccl3$^{-/-}$*. To control for the effects of *Ccl3$^{-/-}$* on non-diseased mice, we

compared the weights of *Ccl3$^{-/-}$; Npc1$^{+/-}$* mice and *Npc1$^{+/-}$* P60 male mice. No gross weight differences were seen at this age (Fig. 2C). Thus, *Ccl3$^{-/-}$* affects weight more notably in *Npc1$^{-/-}$* mice than in *Npc1$^{+/-}$* mice. We also needed to consider genetic backgrounds, which may greatly influence disease progression (44). The *Ccl3$^{-/-}$; Npc1$^{-/-}$* mice were on a mixed FVB and C57BL/6 (B6) background. B6 *Npc1$^{-/-}$* mice life expectancy averages 28–35 days (45), while FVB *Npc1$^{-/-}$* mice live for 72–83 days (35). Despite this marked difference between the two backgrounds, FVB/B6 *Npc1$^{-/-}$* male mice readily survived past P60 and their weights were comparable to FVB *Npc1$^{-/-}$* mice (Fig. 2A, B, D). Thus, we attribute the lower weights

of $Ccl3^{-/-}$; $Npc1^{-/-}$ mice to the $Ccl3$ mutation, not to the background genetic constitution.

Even if other factors were involved in worsening the disease condition of $Ccl3^{-/-}$; $Npc1^{-/-}$ mice, none of the expected weight gains and sustainability demonstrated with the Sandhoff model was observed. In the Sandhoff study (31), $Ccl3^{-/-}$; $Hexb^{-/-}$ mice had higher body weights and ∼30% longer lifespans than $Hexb^{-/-}$ mice. Thus, in contrast to the influence of CCL3 on Sandhoff disease, the endogenous production of CCL3 may play a neutral or beneficial rather than harmful role in NPC disease.

The loss of CCL3 benefited the Sandhoff $Hexb^{-/-}$ mouse model, possibly because it lessened harmful microglia-associated pathology in the CNS and inhibited macrophage infiltration into the CNS. In order to determine whether CCL3 was also required to alter the macrophage and microglia-associated pathology and infiltration in $Npc1^{-/-}$ mice, we quantified the prevalence of CD68-positive cells in both visceral tissue and the CNS. CD68 is a marker of activated microglia and macrophages.

Macrophages do not infiltrate the CNS in NPC-diseased mice

In addition to not improving the weight profile, deleting $Ccl3$ did not alter the prevalence of CD68-positive cells in the CNS of $Npc1^{-/-}$ mice (Fig. 2E and F). Analysis of liver tissues also showed that, in $Ccl3^{-/-}$; $Npc1^{-/-}$ mice, no significant change in CD68 staining was observed. In a few mice, however, enlarged granuloma-like macrophage clusters were present, which may have caused an increase in the average CD68 percentage calculated for the liver (Fig. 2D). The trend towards increased macrophage-associated liver pathology in $Ccl3^{-/-}$; $Npc1^{-/-}$ mice and lack of decrease in CD68-positive cells in the CNS further suggests that endogenous CCL3 may play a neutral or beneficial role in modifying NPC disease pathology.

The main benefit of deleting $Ccl3$ in $Hexb^{-/-}$ mice was suggested to be inhibition of macrophage infiltration into the CNS (31). In order to test whether peripheral macrophages readily invade the CNS of $Npc1^{-/-}$ mice, we labeled or eliminated peripheral macrophages with liposomes (Lp). Dil-label and clodronate-toxin containing Lp (Dil-Lp and Clod-Lp, respectively) have been used extensively in mice to selectively deplete or label macrophages or microglia (41,46,47). When Dil-Lp was injected into the peritoneal cavity of FVB $Npc1^{-/-}$ mice at ages P52 or P70, Dil labeling of CD68-positive macrophage cells was evident in the liver after 24 or 48 h (Fig. 2G). In these same mice, extremely few or no CD68-positive cells were labeled with Dil in the brain. Instead, Dil was sequestered in capillaries after 24 h (Fig. 2H), suggesting that the Dil label is transportable to the brain but that the blood–brain barrier restricted extravasation of Dil-Lp or Dil-Lp-carrying cells. Upon repeated peritoneal injection of Clod-Lp from ages P50–P60, depletion of CD68-positive cells from the liver, but not from the cerebellum, was evident in $Npc1^{-/-}$ mice (Fig. 2I). These results demonstrate that peripheral macrophages do not readily infiltrate and contribute to the CNS pathology in $Npc1^{-/-}$ mice.

The lack of noted macrophage infiltration into the CNS of $Npc1^{-/-}$ mice is distinct from neuroinflammation in $Hexb^{-/-}$ mice, where peripheral macrophages infiltrate the brain and contribute to CNS pathology (31). This difference may be the reason why deletion of CCL3 was not beneficial to $Npc1^{-/-}$ mice. To assess what additional influence CCL3 may have on inflammation and neurodegeneration, we used gene expression profiling to compare $Ccl3^{-/-}$; $Npc1^{-/-}$ and $Npc1^{-/-}$ mice cerebella.

Neuronal NPC1, not deletion of *Ccl3*, suppresses neuroinflammation in NPC-diseased mice

Array analyses of $Ccl3^{-/-}$; $Npc1^{-/-}$ mice compared with age-matched and background-matched $Npc1^{-/-}$ cerebella showed slight decreases in expression of cerebellar Purkinje neuron-specific genes: $Calb1/D28K$, $Pcp2$, $Stk17b/Drak2$, $Fgf7$ and $Gpr63$ (Fig. 3A). Decreased expression of these genes is likely due to reduced numbers of surviving Purkinje neurons (48). $Stk17b$, for example, is produced only in Purkinje neurons of the cerebellum and serves as useful indicator of cell number (Fig. 3C). The expression of Tyrosine hydroxylase (Th) can also be used to assess the condition of Purkinje neurons in the cerebellum in NPC disease since Th is ectopically expressed in cerebellar Purkinje neurons as a consequence of the disease (49). Th levels on average were higher in $Ccl3^{-/-}$; $Npc1^{-/-}$ cerebella than in $Npc1^{-/-}$ mice (Fig. 3A and J). Based in part on the reduction, though slight, of Purkinje neuron-specific genes and mainly on the increase in Th, we conclude that the loss of $Ccl3$ is deleterious to neurons in $Npc1^{-/-}$ mice.

Gene profile array analysis revealed a general increase in expression of genes encoding lysosome-associated proteins, secreted proteases and immune response factors (Fig. 1A) in $Ccl3^{-/-}$; $Npc1^{-/-}$ mice relative to $Npc1^{-/-}$ controls (Fig. 3D and G). The elevation of these inflammatory factors is thought to contribute to neurodegeneration. C1q, a main component of the immune complement pathway, is of particular interest since its production can promote microglial-mediated removal of neuron synapses leading to neuronal death (50). The expression of C1q is elevated early prior to signs of neurodegeneration in NPC disease (12) and here we find that C1q marks cells proximal to Purkinje neuron dendrites in a fashion similar to CD68-positive microglia (Fig. 3F and I). Thus, microglia and C1q-positive cells can be in physical contact with Purkinje neuron dendritic spines to potentially mediate neuron clearance in NPC disease. The increased expression and localization of C1q has been confirmed with RNA probe *in situ* hybridization (data not shown). The increase in C1q and other immune components in $Ccl3^{-/-}$; $Npc1^{-/-}$ mice further suggests that the loss of $Ccl3$ is deleterious to neurons in $Npc1^{-/-}$ mice.

Despite increases in inflammatory factors, the pattern of Purkinje neuron loss and invasion of CD68-positive microglia in $Ccl3^{-/-}$; $Npc1^{-/-}$ mice remains similar to that of $Npc1^{-/-}$ mice. As previously reported (35), CD68-positive microglia are predominantly seen in areas of the cerebellum where Purkinje neurons have degenerated and are absent from areas where they still remain (Supplementary Material, Fig. S2). Thus, eliminating the inflammatory mediator CCL3 did not greatly alter the neurodegenerative process or resulting microglial response. This agrees with the conclusion that CCL3 may play a neutral or beneficial rather than a harmful role in modifying NPC disease.
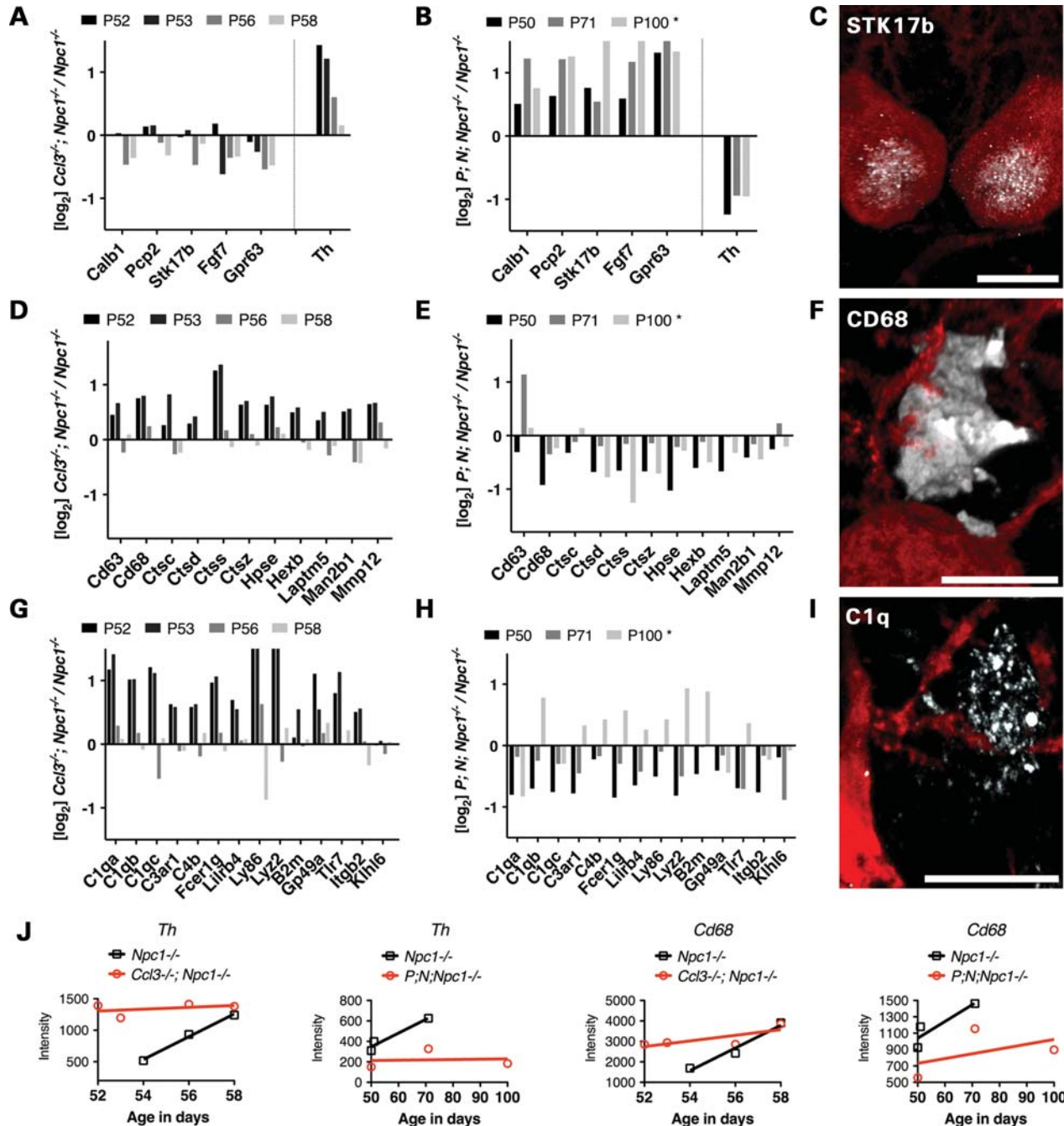
Figure 3. Deletion of *Ccl3* does not retard neurodegeneration or decrease neuroinflammation in NPC mice. (**A**) Microarray analysis between age-matched *Ccl3$^{-/-}$; Npc1$^{-/-}$* and *Npc1$^{-/-}$* FVB/B6 mice at various ages revealed a decrease or limited change in Purkinje neuron-specific genes and a general increase in *Th*. (**B**) In contrast, microarray analysis between age-matched *P; N; Npc1$^{-/-}$* and *Npc1$^{-/-}$* FVB mice showed an increase in Purkinje neuron-specific genes and consistently reduced *Th* RNA. *P; N; Npc1$^{-/-}$* mice at age P100 were compared with *Npc1$^{-/-}$* at P50, since *Npc1$^{-/-}$* mice normally do not survive past age P85. (**C**) As an example of Purkinje neuron specificity, confocal microscopy revealed STK17b protein (white) localized to the nuclear region of Purkinje neurons immunostained with anti-D28K/CALB1 (red). In addition to increased *Th*, microarray analyses of *Ccl3$^{-/-}$; Npc1$^{-/-}$* mice compared with controls revealed increases in (**E**) lysosomal and protease-related genes and (**G**) complement and immune response genes. (**E** and **H**) The expression of these neuroinflammatory components was substantially reduced in *P; N; Npc1$^{-/-}$* mice. (**F**) Anti-CD68 highlighted microglia (white) encompassing Purkinje neuron dendrites (red). (**I**) Similarly, C1q immunofluorescence (white) dotted cell bodies could also be found in close proximity to Purkinje neuron dendrites (red). Confocal image stacks were rendered in 3-D (**F**–**I**). Scale bars are 10 µm. (**J**) The trends for *Th* and *Cd68* array data points are shown.

In a prior study, we reported that patterned Purkinje neuron loss and microglial activity can be halted by neuron-specific production of NPC1 in *P; N; Npc1$^{-/-}$* mice (35). Here, we assessed whether inflammatory factors in general can be suppressed in NPC disease, without eliminating pro-inflammatory components, such as CCL3. We performed gene profiling array analysis on *P; N; Npc1$^{-/-}$* mice, which have early and constitutive production of a functional
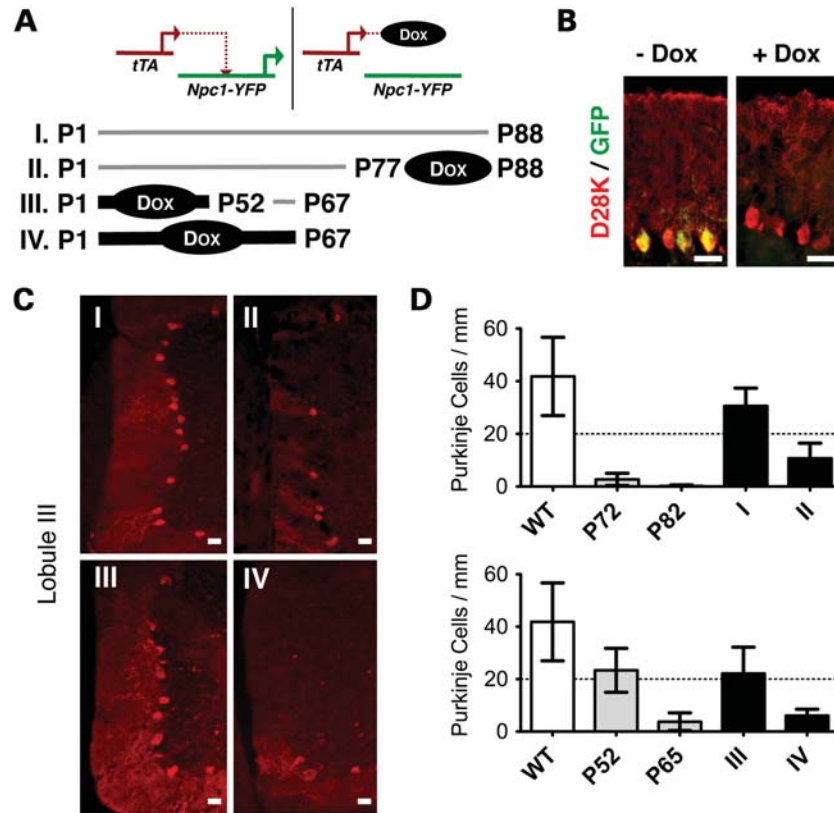
Figure 4. Neuronal survival remains intrinsically regulated despite the age of NPC-diseased mice. (**A**) Expression of the *NPC1-YFP* transgene in *P; N; Npc1$^{-/-}$* was constitutively driven by *Pcp2-tTA* and could be inhibited by Dox applied at different ages (trials I–IV). (**B**) Example of cerebellar Purkinje neurons that normally would produce NPC1-YFP in a *P; N; Npc1$^{+/-}$* mouse showed no detectable NPC1-YFP immunofluorescence enhanced by anti-green fluorescent protein (GFP) in the lobule III region of the cerebellum after Dox was given for over a week. Image is representative of results from four mice. (**C**) Depiction of the difference in the number of surviving Purkinje neurons stained with D28K (red) per trial in cerebellar lobule III. (**D**) Representative quantitative analysis of the number of remaining neurons in lobule III at a given age and per trial. Two mice were used per trial and trials (top graph) I, II, (bottom graph) III and IV were performed in duplicate. The number of Purkinje neurons for wild-type (WT) mice (white bars are the same for each graph) was calculated by averaging together *Npc1$^{+/-}$* mice of approximate ages: P50, P60 and P70. For *Npc1$^{-/-}$* mice of the following ages: P52, P65, P72 and P82 (gray bars are graphed for each age), three or more mice were sampled for each age. Scale bars are 50 μm.

NPC1-YFP protein in cerebellar Purkinje neurons (35). The specific localization of YFP immunofluorescence in Purkinje neuron cell bodies, the reduction in filipin cholesterol stain in Purkinje neurons, and the prevention of increased glial re-activity only in the cerebellum helped confirm that the rescue specifically affected only those cells (35).

Compared with *Ccl3* gene deletion, neuron-specific correction of NPC disease in *P; N; Npc1$^{-/-}$* mice had a considerable and opposite effect on neuroinflammation. Providing NPC1 to Purkinje neurons in *Npc1$^{-/-}$* mice maintained Purkinje neuron-specific gene expression levels and suppressed increases in *Th* (Fig. 3B and J, Supplementary Material, Fig. S3). While *Ccl3* gene deletion tended to increase the levels of inflammation (Fig. 3D, G, J), all inflammatory factors identified by array, including *C1q,* were suppressed in the cerebella of *P; N; Npc1$^{-/-}$* mice (Fig. 3E and H). This demonstrates that much of the abnormal inflammatory gene expression in the cerebella of *Npc1$^{-/-}$* mice results from neuronal defects that stimulate inflammatory cells, rather than the loss of NPC1 from microglia.

The future of therapeutic approaches, genetic or otherwise, for neurodegenerative disorders may depend on arresting the progression of neuronal loss when a patient is already

exhibiting disease signs. For NPC disease, prior studies demonstrated that neuronal NPC1 is required for neuron survival (35,51). However, these studies did not address whether neuronal NPC1 is sufficient to halt neuron loss late in the disease after mice initially develop without NPC1 function. Methods of intrinsic neuron rescue will work only if the early events in the disease do not set in motion an unstoppable process of decay that contributes to non-autonomous neuronal toxicity and elimination. Since neuron rescue and not deletion of *Ccl3* had such a dramatic effect on suppressing inflammation and preventing neuronal loss, we next focused on manipulating the timing of neuron rescue to see whether NPC disease could be arrested or reversed at late stages of the disease.

Arresting neurodegeneration late in NPC disease progression

In order to test whether neuron rescue is possible late in the disease, we regulated the production of NPC1-YFP in *P; N; Npc1$^{-/-}$* mice with Doxycycline (Dox). Dox binds to the tTA protein produced by *Pcp2-tTA* and inhibits its ability to induce the expression of a *tetO-* transgene (Fig. 4A). This method has been previously been used to show

neurodegenerative recovery of Purkinje neurons by inhibiting the continuous expression of mutant *ataxin-1* (52).

First, we tested whether suppression of the production of Purkinje neuron NPC1-YFP in *P; N; Npc1$^{-/-}$* mice with Dox (Fig. 4B) can elicit neurodegeneration. Cerebellar lobule III was chosen for analysis because of its consistent morphology across mice of various ages and its early loss of Purkinje neurons compared with more posterior lobules (53). In male FVB *Npc1$^{-/-}$* mice, Purkinje neuron loss starts to become apparent in lobule III by age P50. By P65, *Npc1$^{-/-}$* mice tend to be devoid of Purkinje neurons in this cerebellar region. In sharp contrast, *P; N; Npc1$^{-/-}$* mice at age P88 have considerably more neurons surviving in the lobule III region of the cerebellum than *Npc1$^{-/-}$* mice older than P72 (Fig. 4C and D-trial I). When Dox is administered continuously to *P; N; Npc1$^{-/-}$* mice starting at P77, neuron loss commences. At P88, *P; N; Npc1$^{-/-}$* mice that had been treated with Dox starting at P77 showed Purkinje neuron loss that resembles the degree of Purkinje neuron loss that occurs in *Npc1$^{-/-}$* mice between P52 and P65 (Fig. 4D-trial II). Thus, removing NPC1 function from neurons of adult *P; N; Npc1$^{-/-}$* mice triggers degeneration of neurons. These data from *Npc1$^{-/-}$* mice support results obtained from *Npc1$^{+/+}$* mice with conditional knockout of the *Npc1* gene in mature neurons (51).

To demonstrate that providing NPC1 function to neurons allows neuron survival even well along in the disease, we administered Dox continuously to *P; N; Npc1$^{-/-}$* mice from birth to P52. Dox was removed at P52. By P52, inflammatory processes have had ample time to intensify (Fig. 1A). When assessed at age P67, these mice did not differ in the amount of Purkinje neurons in lobule III compared with P52 *Npc1$^{-/-}$* mice (Fig. 4D-trial III). Thus, restoring NPC1-YFP production in Purkinje neurons at P52 halted the neurodegenerative process (Fig. 4C and D). If Dox was not removed at P52, then the number of Purkinje neurons remaining in lobule III at P67 in *P; N; Npc1$^{-/-}$* mice was not significantly different ($P = 0.333$ $n = 4$ mice) than the number of Purkinje neurons typically remaining at P65 in *Npc1$^{-/-}$* mice (Fig. 4D-trial IV). Thus, neuronal NPC1 function is necessary for the survival of neurons and sufficient to arrest neurodegeneration.

Since neuron survival can be controlled even at late stages of the disease without eliminating inflammatory mediators in *Npc1$^{-/-}$* mice, we hypothesized that other cell types vulnerable to the disease could be rescued without targeting macrophages or immune cells in the body. NPC disease is a complex disorder that affects multiple tissues in addition to the nervous system. Notably, liver and pulmonary injuries are leading causes of death of NPC patients (54–56). If macrophage-associated pathology in visceral tissue operates in a fashion similar to microglia-associated pathology in the CNS, then correction of hepatic cells in the liver, for example, should be sufficient to suppress the inflammation even after tissue pathology has become severe.

Reversing macrophage-associated NPC-diseased tissue pathology

To test whether liver rescue is possible late in the disease, we regulated the production of NPC1-YFP with the *ROSA26r-rtTA-M2* transgene (R) in *R; N; Npc1$^{-/-}$* mice

(35). rtTA is regulated in the opposite way from tTA; Dox binding to rtTA induces expression of the tetO transgene (Fig. 5A). It is also known that the *ROSA26r-rtTA-M2* transgene, in the presence of Dox, induces expression of a tetO transgene in fibroblasts and epithelial cells throughout the body (57). Thus, in addition to being able to time NPC rescue in visceral tissue of *R; N; Npc1$^{-/-}$* mice, we were also able to selectively test the importance of NPC1 function in epithelial cells of various organs in the context of NPC1-deficient immune cells.

We found that the production of the NPC1-YFP protein was inducible by Dox in non-macrophage cells both *in vitro* and *in vivo*. *In vitro*, addition of Dox to culture media can induce NPC1-YFP in primary fibroblasts but not in peritoneal cells isolated from *R; N; Npc1$^{-/-}$* mice (Fig. 5B). *In vivo*, when *R; N; Npc1$^{-/-}$* mice were fed Dox, NPC1-YFP was produced in the liver and detected by immunofluorescence (Fig. 5B and C). In these Dox-treated *R; N; Npc1$^{-/-}$* mice, resident macrophages and invading monocytes or lymphocytes in the liver did not have detectable NPC1-YFP protein. NPC1-YFP immunofluorescence was also absent from the spleen and restricted to a few cells in the thymus and bone marrow that are not Thy1.2 positive (Fig. 5C and D). Thus, NPC1-YFP was produced broadly in visceral tissue of *R; N; Npc1$^{-/-}$* mice but was largely absent from monocytes, lymphocytes and bone marrow cells.

Despite the lack of NPC1-YFP rescue in macrophages, cholesterol accumulation in the liver of *R; N; Npc1$^{-/-}$* mice was modified after a week of NPC1-YFP induction (Fig. 5E). Although some filipin stain persisted, it was now in individual cells dispersed throughout the liver. These cells lacked NPC1-YFP immunofluorescence and were identified as predominantly macrophages based on CD68 staining (Fig. 5F). High-magnification imaging showed that macrophages in liver tissue of *R; N; Npc1$^{-/-}$* mice had changed from a foam cell appearance to a more ramified intermediate state once liver epithelial cells or hepatocytes were genetically rescued (Fig. 5G). With prolonged NPC1-YFP induction, the majority of macrophages in the livers of *R; N; Npc1$^{-/-}$* mice shared a resting state morphology equivalent to macrophages found in wild-type mice. Thus, macrophages in liver remained responsive to their environment despite having a continuous NPC1 defect.

Focal macrophage responses to changes in local environments within the same tissue can be seen upon brief (3–5 days) induction of NPC1-YFP in P65 or older *R; N; Npc1$^{-/-}$* mice. In the liver, foam cell macrophages clustered in localized non-rescued liver areas, marked by lack of green fluorescent protein (GFP) immunofluorescence and intense filipin stain (Fig. 6A). Those areas may have been sites of severe liver tissue injury, containing cells other than hepatocytes that do not produce NPC1-YFP.

In lungs, a localized macrophage response was also seen. Macrophages near simple squamous epithelial cells producing NPC1-YFP had drastically thin morphology compared with the large foam cell morphology of macrophages near lung epithelia lacking NPC1-YFP (Fig. 6B). The macrophage morphology change in lung was roughly quantified by the percent of alveolar tissue area occupied by CD68 immunofluorescence. No change in morphology occurred in macrophages located
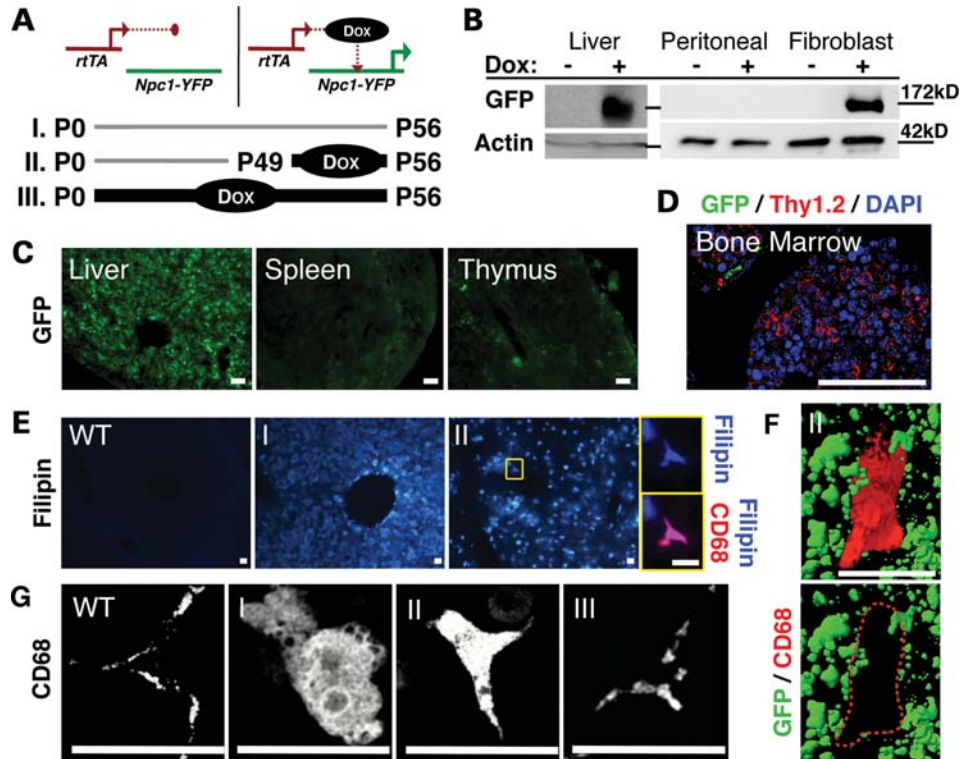
Figure 5. Macrophage-associated NPC liver pathology is corrected without immune cell rescue. (**A**) Expression of the NPC1-YFP transgene, driven by *Rosa-rtTA* in *R; N; Npc1*$^{-/-}$ mice, can be induced with Dox at different ages (trials I–III). (**B**) Immunoblotting with anti-GFP demonstrated that, upon Dox induction, NPC1-YFP protein was detected in liver tissue and cultured skin fibroblast cells but not in isolated peritoneal cells. Representative data from three animals are shown. (**C**) Immunofluorescence with anti-GFP detected NPC1-YFP above tissue autofluorescence in liver but not in spleen, and in limited areas of the thymus. (**D**) Confocal imaging showed that NPC1-YFP immunofluorescence did not colocalize with Thy1.2-positive cells in isolated bone marrow cell clusters. These expression patterns (C and D) were observed for all mice used in this study. (**E**) Upon brief 1-week Dox induction of NPC1-YFP, reduced cholesterol accumulation was seen in liver sections except in macrophages (yellow square and magnified view). (**F**) Confocal 3-D rendering demonstrated the absence of NPC1-YFP (green isosurface) in a representative CD68-positive cell (red) in the liver. (**G**) With prolonged Dox-induced NPC1-YFP, the population of foamy CD68-positive cells reverted to a more ramified normal morphological appearance. Images of single CD68-positive cells are representative of >50% of the cells in the tissue. Each trial, I–III, included a minimum of five mice. Scale bars are 50 μm.

away from sites of maximum NPC1-YFP production in the alveoli, which happened to be bronchioles (Fig. 6C and D). These results demonstrate, for the first time, reversal of abnormal macrophage behaviors in the lung of *Npc1*$^{-/-}$ mice.

Taken together, our rescue experiments in the brain, liver and lung suggest that macrophage abnormalities in NPC are driven by abnormal local tissue environments and not due to intrinsic defects in NPC1 production. To more directly ascertain the relative contribution of immune cells to NPC pathology, we pharmacologically depleted macrophages from the viscera and compared liver injury with amount of liver injury that resulted from hepatocyte epithelial cell rescue or *Ccl3* deletion.

Macrophage intervention is not required for reducing tissue injury in NPC-diseased mice

Deletion of the macrophage inflammatory cytokine *Ccl3* from *Npc1*$^{-/-}$ mice (Fig. 7A) did not reduce the levels of the hepatic enzyme alanine aminotransferase (ALT) in the blood (Fig. 7D). Serum levels of ALT serve as a clinical marker of hepatocyte injury, so we conclude that liver damage was not reduced in *Ccl3*$^{-/-}$; *Npc1*$^{-/-}$ mice. A separate study also

observed that ALT levels were not reduced in a mouse knockout of the cytokine tumor necrosis factor (TNF)-alpha when NPC liver disease was induced with NPC1-specific antisense oligonucleotides (58). Despite little difference in ALT levels, the authors noted that the loss of TNF-alpha delayed macrophage-associated pathology in the liver. In our study, ALT levels did correlate with the degree of macrophage-associated liver pathology caused by deletion of *Ccl3* (Figs 2E and 7D). Given these reported phenotypes, it remains uncertain whether macrophage activity in the liver can be toxic to hepatocytes.

To explore the relevance of macrophages to liver injury, we depleted liver macrophages from *Npc1*$^{-/-}$ mice using Clod-Lp (Fig. 7B). Although repeated Clod-Lp injections caused some toxicity, evident as a small increase in ALT levels in non-NPC animals, if macrophage activity is harmful in NPC disease the resulting smaller macrophage population should have lessened liver injury in *Npc1*$^{-/-}$ mice. Instead, we saw an average increase in ALT levels (Fig. 7E).

Serum ALT levels in *Npc1*$^{-/-}$ mice have been reduced only when treatments targeted the storage accumulation in the liver (27,54). These treatments, such as CYCLO, were not cell-specific and thus have not revealed the cell type responsible
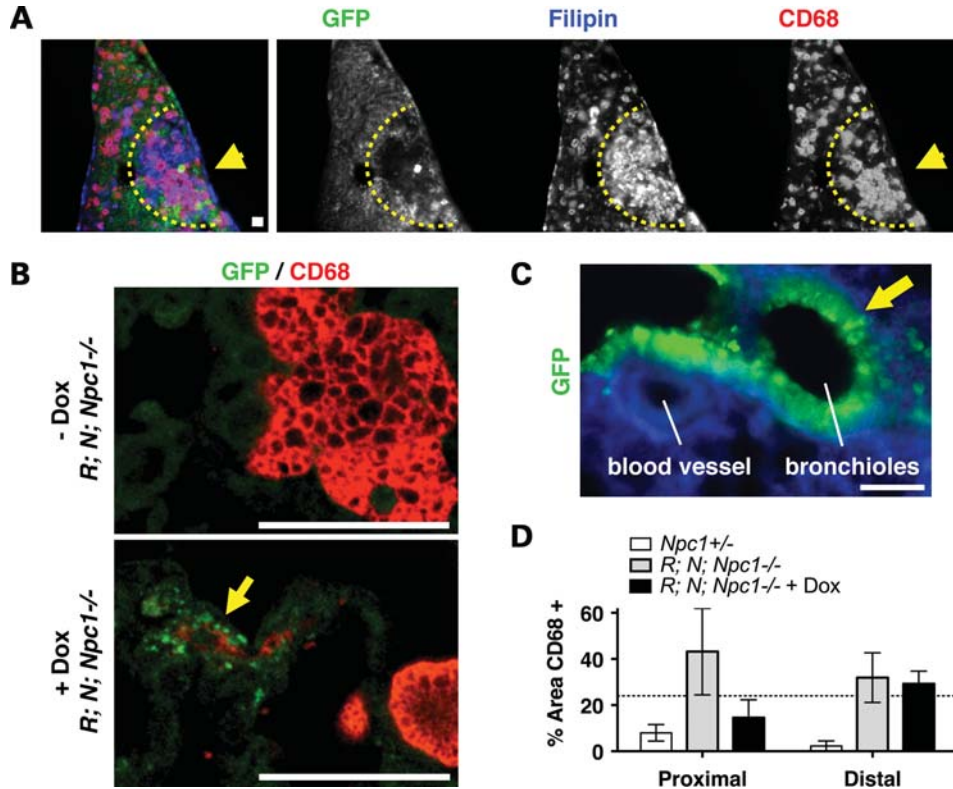
Figure 6. Macrophages respond locally to epithelial cell rescue. (**A**) Dox administered to P65 or older *R; N; Npc1*$^{-/-}$ mice produced a mosaic rescue effect in liver tissue. Regions (inside semi-circle) that did not produce NPC1-YFP immunofluorescence (GFP, green) remained cholesterol positive (Filipin, blue) and had focal accumulation (arrow) of clustered macrophages (CD68, red). (**B**) In lung alveoli, foam cell CD68-positive macrophages (red) were seen proximal to simple squamous epithelial cells (top panel). Macrophages near simple squamous epithelial cells producing NPC1-YFP (bottom panel, yellow arrow) were reduced in size in comparison to the large foam macrophages surrounding non-NPC1-YFP-positive epithelial regions. (**C**) Apart from a few sparse squamous cells, NPC1-YFP immunofluorescence predominated in the epithelial linings (arrow) of bronchioles in *R; N* mice given Dox. (**D**) Quantification of the percent area that was CD68 positive in alveoli shows a significant ($P = 0.0061$, $n = 3$ mice) decrease in CD68 in alveoli regions most proximal to bronchioles. Scale bars are 50 μm.
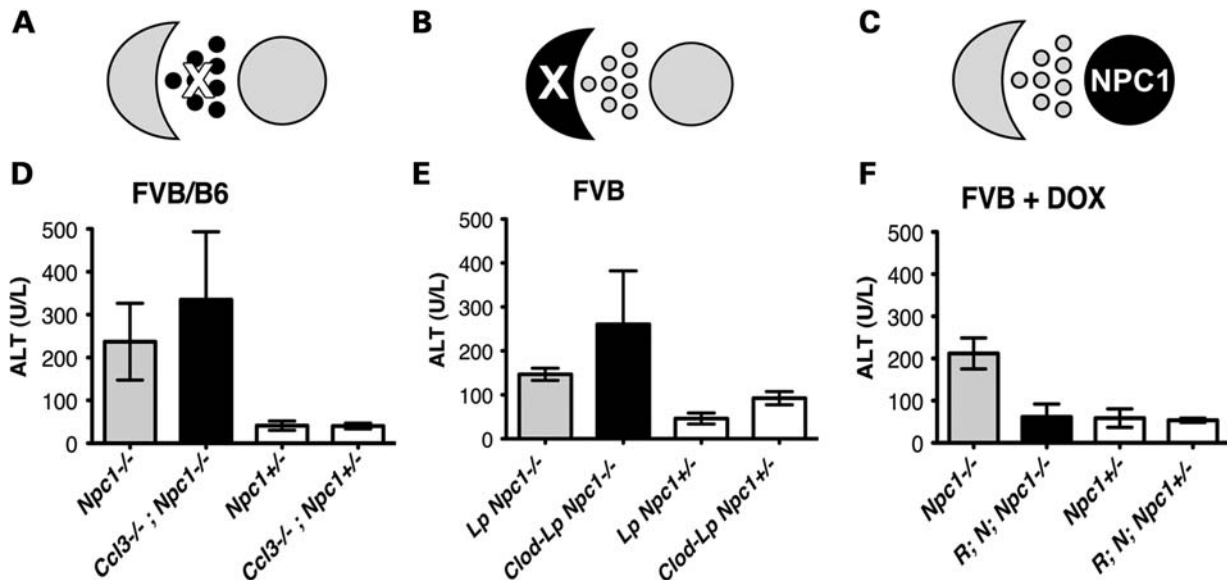

Figure 7. Serum ALT levels are elevated in the absence of Ccl3 and macrophages but reduced when NPC1 is provided to hepatocytes. Depictions of treatment target in liver of NPC mice. (**A**) Genetic deletion of cytokine *Ccl3*. (**B**) Depletion of peripheral macrophages. (**C**) NPC1 provision to hepatocytes. ALT blood levels show (**D**) an average but not significant increase in ALT levels from *Ccl3*$^{-/-}$; *Npc1*$^{-/-}$ compared with *Npc1*$^{-/-}$ FVB/B6 mice at age P58, (**E**) an average but not significant increase in ALT levels from Clod-Lp-treated *Npc1*$^{-/-}$ compared with control Lp-treated *Npc1*$^{-/-}$ FVB mice at age P56, and (**F**) an average and statistically significant decrease ($P = 0.0055$) in ALT levels from Dox-treated *R; N; Npc1*$^{-/-}$ compared with Dox-treated *Npc1*$^{-/-}$ FVB mice at age P56. Minimum of four mice was used for each ALT analysis.
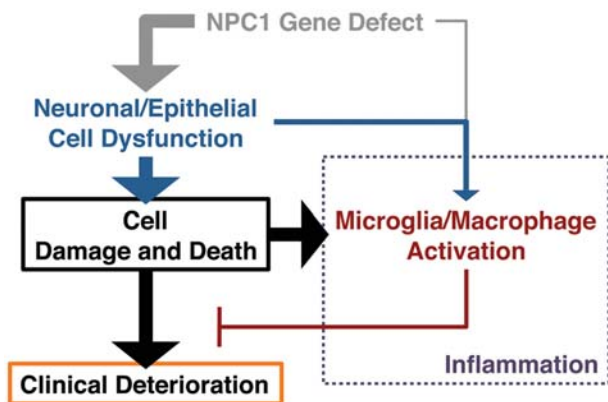
Figure 8. Proposed roadmap of NPC pathogenesis. Model for acute neurode-generation and tissue injury in the lysosomal storage Niemann-Pick disease type C. Line thickness represents degree of involvement.

for the beneficial effect. Using *R; N; Npc1*$^{-/-}$ mice, we found that genetically providing NPC1 function to epithelial cells in the liver, but not macrophages (Fig. 7C), for a week was sufficient to normalize serum levels of ALT (Fig. 7F). Thus, hepatic injury, like neuron injury, is primarily due to the absence of NPC1 in the cell itself and not to an aberrant inflammatory response or abundant immune cell activity.

DISCUSSION

Our experiments indicate that inflammation in the NPC mouse model of LSD resembles a self-limiting inflammatory reaction. Inflammation is described as self-limiting or acute when it continues only until the threat to the cell is eliminated and tissue homeostasis is restored (59). In *Npc1*$^{-/-}$ mice, we demonstrate that correcting neuronal or epithelial cells is sufficient to suppress inflammation and reverse the macrophage-associated pathology in tissues (Figs 3, 5 and 6). Furthermore, neuron loss and tissue injury could be halted, even late in NPC disease, if neurons and epithelial cells were treated before the cells were lost (Figs 4 and 7). Although the NPC1 defect remains in macrophages and other immune cells, we find that this does not preclude resolution of inflammation in NPC disease. The inflammatory response remains a secondary response to tissue injury. This is encouraging news for modifying the disease progression of NPC patients, even if diagnosis or treatment of the disease occurs later in life.

Surprisingly, attempts to perturb the inflammatory response by genetically deleting the macrophage inflammatory cytokine *Ccl3* or depleting activated macrophages from tissues in *Npc1*$^{-/-}$ mice proved more deleterious than beneficial as a therapeutic approach (Figs 2, 3 and 7). These results provide evidence that the inflammatory activity of microglia and macrophages in NPC disease in response to cell defects and injury may be a beneficial adaptation to try and prevent excessive tissue damage (Fig. 8). This view is supported by recent *in vitro* data demonstrating that abundant *Npc1*$^{-/-}$ microglia promote neuron survival of wild-type neurons in microglia-neuron co-cultures (60). Whether similar events occur in

other LSDs has yet to be explored in sufficient detail and in appropriate models.

Deletion of *Ccl3* allowed us to determine the relevance of this cytokine to NPC disease progression and to experimentally bridge NPC disease with the LSD Sandhoff disease. Our results highlight an important distinction between NPC and Sandhoff disease mouse models with regards to inflammation. For the *Npc1*$^{-/-}$ mouse model of NPC disease, we now have multiple lines of evidence to show that the degeneration of neurons is governed by neuron-intrinsic defects. The elevation of the inflammatory response itself does not drive elimination of healthy neurons (Figs 3 and 4) and macrophage infiltration into the CNS is not seen (Fig. 2). In the *Hexb*$^{-/-}$ mouse model of Sandhoff disease, in contrast, macrophage invasion into the CNS has been shown, and neuronal defects and inflammation are proposed to converge to promote neurodegeneration (31). To date, the pathogenic cascade of the Sandhoff disease model has been the most widely proposed pathogenic cascade for lysosomal storage diseases in general (1–3). The distinct roles of inflammation in NPC and Sandhoff diseases, however, argue for reevaluating the roles of neuroinflammation in other LSDs that have neurological deficits.

Functional differences among LSDs may be concealed behind overtly similar phenotypes, such as visible accumulations of lysosome material or elevation of inflammatory components. NPC and Sandhoff both accumulate glycosphingolipids (33), which are potent immune modulators, yet the same genetic treatment that benefitted the Sandhoff mouse model was deleterious to NPC mice (Figs 2 and 3). NPC, Sandhoff and other LSDs also share multiple elevated pro-inflammatory cytokines (37,38), yet the influence of these cytokines may differ between disease states. Differences in the roles of inflammation among LSDs may be better determined by properties specific to the pathways and cell types involved. Thus, the role of inflammatory cells has to be carefully analyzed for an individual LSD and, if possible, the cell types therapeutically relevant to treating the disease identified in order to begin to categorize LSDs based on treatment potential.

Unlike lysosomal storage disorders that are caused by loss of function of a secretable enzyme, NPC disease caused by loss of transmembrane protein NPC1 function is cell autonomous. Providing NPC1 to one cell does not correct the defect in another (35,53,61). Along with cell autonomy, NPC disease also demonstrates tissue autonomy between organ systems, so that an alteration, such as reduced inflammation, in one system or tissue area does not necessarily modify the pathology in another. This is in contrast to the non-cell-autonomous neurodegenerative mSOD1 mouse model of amyotrophic lateral sclerosis, where immune modulation in peripheral tissues such as the liver could potentially result in a global neuroprotective intervention (62). For a cell-autonomous neurodegenerative disease such as NPC, global pathology is unlikely to be corrected by selective treatment of specific tissues. Tissue autonomy in NPC disease is demonstrated by the observation that peripheral monocytes do not invade the brain in *Npc1*$^{-/-}$ mice (Fig. 2) and the macrophage pathology in liver and lung can be locally reduced depending on where in the tissue NPC1 is produced (Figs 5 and 6). As a result, genetic or environmental risk

factors as well as therapeutic applications that affect a particular tissue system will elicit a modified clinical phenotype only within the target tissue despite a similar NPC1 gene defect throughout the body.

Future NPC research directions should focus on identifying modifiers of the disease in order to better understand the variability in visceral tissue pathology seen in human patients (63). Although late NPC disease pathology can be mitigated (Figs 5–7), genetic variables and early developmental attributes still appear to contribute to how the disease progresses. The altered disease progression reflected by weight measurements of $Ccl3^{-/-}$; $Npc1^{-/-}$ mice (Fig. 2) suggests that pre-existing differences in the cytokine milieu can contribute to disease severity, particularly in visceral tissue. Other factors, genetic and environmental may also be involved (64).

Our results demonstrate that $Npc1^{-/-}$ macrophages and immune cells respond appropriately to epithelial and neuronal injury in NPC disease and that targeting cytokines produced by macrophages or depleting macrophages in NPC disease may inadvertently promote peripheral tissue or neuronal injury. These characteristics of NPC disease pathology have implications beyond NPC and the LSD research community and may help treat disparate diseases, especially human immunodeficiency virus (HIV) and Ebola virus infection. The processes of HIV and Ebola virus infection has been linked to NPC disease through function of the NPC1 protein. Loss of NPC1 alters transmission of HIV by affecting its packaging and excretion from the infected cell (10). Loss of NPC1 limits Ebola virus transmission by trapping Ebola in endocytic compartments of host cells, thereby preventing infection (65). In both viral diseases, macrophages and lymphocytes are believed to be the main reservoirs of the viruses and facilitate virus transmission throughout the body. Based on the findings reported here, inhibition of NPC1 function in macrophages and immune cells could help moderate HIV and Ebola viral infection without eliciting neurodegeneration or causing much tissue injury.

MATERIALS AND METHODS

Transgenic mice

Care and handling of mice was in accordance with institutional guidelines. Mice homozygous for the *Ccl3*-targeted mutation (JAX Mice Strain Name: B6.129P2-*Ccl3^{tm1Unc}*/J) were obtained from The Jackson Laboratory. These C57BL/6 $Ccl3^{-/-}$ mice were crossed to congenic FVB $Npc1^{-/-}$ mice (originally JAX Mice Strain Name: BALB/cNctr-*Npc1^{m1N}*/J) previously generated in our laboratory (35). Offspring genotyped as $Ccl3^{+/-}$; $Npc1^{+/-}$ was bred to produce experimental $Ccl3^{-/-}$; $Npc1^{-/-}$ mice and controls, $Npc1^{+/-}$, $Npc1^{-/-}$ and $Ccl3^{-/-}$; $Npc1^{+/-}$ mice of mixed FVB/B6 background. The genotypes of the *Ccl3* and *Npc1* loci were determined by PCR of genomic DNA obtained from ear clips. Primers to detect the mutations in the *Ccl3* and *Npc1* loci have been previously described (31,35). Reverse transcription (RT)–polymerase chain reaction (PCR) of liver total RNA was performed on half of the $Ccl3^{-/-}$; $Npc1^{-/-}$ mice generated in order to confirm loss of *Ccl3* mRNA. A primer pair was used to generate a 433 bp amplicon as follows: 5′-CCTCTGTCACCTGCTCAACATC-3′

and 5′- ATGTGGCTACTTGGCAGCAAAC-3′. *Actin* primer pairs for control PCR, 5′-GCTCCGGCATGTGCAAAG-3′ and 5′-CCTCGGTGAGCAGCACAG-3′, generate a ~283 bp amplicon.

For humane reasons, mice were sacrificed under regulated CO_2 if lethargic and the body weight of a NPC-diseased mouse dropped below 14 g for male mice or 12 g for female mice older than P40. Weight measurements were made every 2–7 days, or at ages reported. *P; N; $Npc1^{-/-}$* and *R; N; $Npc1^{-/-}$* mice were generated in our laboratory as previously described (35).

Liposome treatment

Clodronate- and Dil-containing liposomes, as well as empty vehicle liposomes, were purchased from Encapsula NanoSciences. Approximately 200 μl of Dil-Lp solution was injected into the peritoneal cavity of FVB P52 or P70 $Npc1^{-/-}$ mice. Liver and brain tissue was dissected and analyzed 24–48h later. Approximately 100 μl of Clod-Lp or control Lp solution was injected into the peritoneal cavity of FVB $Npc1^{-/-}$ and wild-type mice at days P49 and P53. Liver and brain analyses were performed at P56.

Dox treatment

Mice were given Dox hyclate (Sigma) at a concentration of 2 mg/ml in their drinking water with 5% sucrose. The solution was refreshed every 3 days and light-protected water bottles were used. For *R; N; $Npc1^{-/-}$* mice, induction of NPC1-YFP was confirmed by skin biopsy. The NPC1-YFP fluorescence produced by fibroblast skin cells in the biopsy can be detected by standard fluorescent microscopy using a ×20 objective and GFP filter set.

Liver ALT

ALT plasma level analysis was performed in-house at the Stanford University Veterinary Service Center. $Ccl3^{-/-}$; $Npc1^{-/-}$ mice ALT was measured at age P58. Clod-Lp- and Lp-treated mice ALT was measured at P56. For *R; N; $Npc1^{-/-}$* mice, ALT levels were measured at P56 after mice were given Dox for 7 days.

Gene profiling

Cerebella from $Ccl3^{-/-}$; $Npc1^{-/-}$ mice and sibling $Npc1^{-/-}$ mice, *P; N; $Npc1^{-/-}$* mice and age-matched $Npc1^{-/-}$ mice, or $Npc1^{-/-}$ and $Npc1^{+/-}$ mice were harvested and total RNA was extracted with Trizol reagent (Invitrogen). A total of 16 animals were used. Individual arrays were performed on total RNA from each whole cerebellum isolated. Genomic DNA was removed with Turbo DNA-free kit (Ambion) and the RNA further purified with Acid Phenol:ChCl₃ (Ambion) and subsequent alcohol precipitation steps. A quality check of RNA by Agilent Bioanalyzer QC, cDNA synthesis, hybridization onto Affymetrix GeneChip® Mouse Gene 1.0 ST Arrays and scanning was performed at Stanford Protein and Nucleic Acid Facility. Normalized intensity data were obtained using the Affymetrix Expression Console software and RMA

default settings. Intensity values and raw microarray data were deposited in NCBI's Gene Expression Omnibus (66) and can be viewed through GEO Series accession number GSE36119. Known genes showing a 2-fold or greater increase in $Npc1^{-/-}$ compared with $Npc1^{+/-}$ FVB mice at P50 were ranked based on averages. SAM assessed significance and the functional groupings (Fig. 3) of the top ∼50 genes (Fig. 1) were assigned using the Database for Annotation, Visualization and Integrated Discovery (DAVID) (67).

Low-cycle RT–PCR analysis of *Ccl3* RNA levels was performed on total RNA isolated from various tissues and brain regions of P60 $Npc1^{-/-}$ and $Npc1^{+/-}$ mice. The *Ccl3* and *Actin* primer pairs are noted above, under Transgenic Mice section.

Immunofluorescence, staining and quantification

Primary antibodies used in this study: chicken anti-GFP (Aves), chicken anti-Glial fibrillary acidic protein (GFAP) (Aves), chicken anti-Tyrosine Hydroxylase (Aves), rabbit anti-Calbindin/D28K (Sigma), rat CD68 (Abdserotec), rabbit anti-DRAK2 (Cell Signaling Technology), Thy1.2 (abcam), rat C1q (abcam) and mouse anti-Actin (Millipore). Appropriate Alexa and horseradish peroxidase (HRP)-conjugated secondary antibodies were obtained from Invitrogen and Jackson ImmunoResearch. Filipin (Sigma) was added with secondary antibodies during staining.

For tissue immunofluorescence microscopy, all tissues were isolated and fixed overnight in 4% paraformaldehyde phosphate buffer saline (PBS) solution at 4°C, then sectioned with a Vibratome into 50 μm slices. Brains were sectioned sagitally. Bone marrow was extruded into fixative. Tissue sections and bone marrow clumps were incubated with primary antibody overnight at 4°C in 2% bovine serum albumin (BSA)/0.2% Triton X-100 PBS blocking solution. For tissue treated with Dil-Lp, 2% BSA/0.1% Tween-20 PBS blocking solution was used to preserve Dil localization. Blocking solutions were used for washes at room temperature and secondary incubation at 4°C overnight followed by additional room temperature washes. Tissue sections were mounted and sealed onto slides. Bone marrow cells were pelleted and spread on slides.

Epifluorescent images were obtained using a Zeiss Axioplan2 fluorescent microscope equipped with an AxioCam HRc CCD camera. A 10% neutral density filter was used to prevent photobleaching of filipin stain. Confocal images were obtained with a Leica TCS SP2 laser-scanning microscope. Images were processed and rendered using the Volocity imaging software. Quantification of the percent area of tissue occupied by CD68 immunofluorescence was measured using the ImageJ software as previously described (35).

Cell isolation and immunoblot analysis

Peritoneal cells were isolated by syringe injecting 7 ml of cold PBS into the peritoneal cavity of a euthanized mouse and aspirating back up 5 ml. Suspended peritoneal cells were centrifuged at 1000g for 5 min and PBS was replaced with the complete growth medium and Dulbecco's modified Eagle medium (DMEM) (Gibco) with 10% fetal bovine serum (FBS) (Thermo Scientific). Resuspended cells were allowed to settle onto a plastic surface for 6 h. Remaining debris was gently washed off. Dox was added to the remaining cells at a concentration of 100 ng/ml for 48 h before immunoblotting procedure. For RT–PCR analysis, freshly isolated peritoneal cells were pelleted and placed in Trizol for RNA extraction.

Primary fibroblast cells were cultured in complete medium, DMEM with 10% FBS supplemented with normocin (Invivogen), from tail biopsies of adult $R; N; Npc1^{-/-}$ mice. Finely diced tail segments were seeded onto tissue culture plates with low-level media to prevent floating of segments away from floor of the plate. Partial media exchange was performed daily until cell colonies beside large tissue pieces were seen. Remaining tissue bits were removed and colony forming cells were expanded. Dox was added to the remaining cells at a concentration of 100 ng/ml for 48 h before immunoblotting procedure.

For immunoblotting, equal numbers of cells or mass of liver tissue were lysed in cold radioimmunoprecipitation assay buffer supplemented with complete EDTA-free protease inhibitor cocktail mini tablets (Roche). Cells or tissue were homogenized with motorized pestle. Insoluble material was pelleted at 10 000g for 10 min. Supernatants were stored in Laemmli protein sample buffer prior to electrophoresis in gradient gels (Bio-Rad, Invitrogen). Primary antibodies were incubated overnight at 4°C in 2% BSA/0.2% Tween-20 PBS solution. HRP-conjugated secondary antibodies were incubated at room temperature for 30 min. The HRP chemiluminescence produced by adding SuperSignal West Pico Chemiluminescent Substrate (ThermoScientific) was imaged using a ChemiDoc XRS System (Bio-Rad).

SUPPLEMENTARY MATERIAL

Supplementary Material is available at *HMG* online.

Conflict of Interest statement. None declared.

FUNDING

REFERENCES

1. Castaneda, J.A., Lim, M.J., Cooper, J.D. and Pearce, D.A. (2008) Immune system irregularities in lysosomal storage disorders. *Acta Neuropathol.*, **115**, 159–174.
2. Vitner, E.B., Platt, F.M. and Futerman, A.H. (2010) Common and uncommon pathogenic cascades in lysosomal storage diseases. *J. Biol. Chem.*, **285**, 20423–20427.
3. Futerman, A.H. and van Meer, G. (2004) The cell biology of lysosomal storage disorders. *Nat. Rev. Mol. Cell Biol.*, **5**, 554–565.

4. Jeyakumar, M., Dwek, R.A., Butters, T.D. and Platt, F.M. (2005) Storage solutions: treating lysosomal disorders of the brain. *Nat. Rev. Neurosci.*, **6**, 713–725.

5. Parkinson-Lawrence, E.J., Shandala, T., Prodoehl, M., Plew, R., Borlace, G.N. and Brooks, D.A. (2010) Lysosomal storage disease: revealing lysosomal function and physiology. *Physiology (Bethesda)*, **25**, 102–115.

6. Pressey, S.N., Smith, D.A., Wong, A.M., Platt, F.M. and Cooper, J.D. (2012) Early glial activation, synaptic changes and axonal pathology in the thalamocortical system of Niemann-Pick type C1 mice. *Neurobiol. Dis.*, **45**, 1086–1100.

7. Vanier, M.T. (2010) Niemann-Pick disease type C. *Orphanet J. Rare Dis.*, **5**, 16.

8. Kaye, E.M. (2011) Niemann-Pick C disease: not your average lysosomal storage disease. *Neurology*, **76**, 316–317.

9. Maxfield, F.R. and Tabas, I. (2005) Role of cholesterol and lipid organization in disease. *Nature*, **438**, 612–621.

10. Tang, Y., Leao, I.C., Coleman, E.M., Broughton, R.S. and Hildreth, J.E. (2009) Deficiency of niemann-pick type C-1 protein impairs release of human immunodeficiency virus type 1 and results in Gag accumulation in late endosomal/lysosomal compartments. *J. Virol.*, **83**, 7982–7995.

11. Sagiv, Y., Hudspeth, K., Mattner, J., Schrantz, N., Stern, R.K., Zhou, D., Savage, P.B., Teyton, L. and Bendelac, A. (2006) Cutting edge: impaired glycosphingolipid trafficking and NKT cell development in mice lacking Niemann-Pick type C1 protein. *J. Immunol.*, **177**, 26–30.

12. Liao, G., Wen, Z., Irizarry, K., Huang, Y., Mitsouras, K., Darmani, M., Leon, T., Shi, L. and Bi, X. (2010) Abnormal gene expression in cerebellum of Npc1-/- mice during postnatal development. *Brain Res.*, **1325**, 128–140.

13. Infante, R.E., Abi-Mosleh, L., Radhakrishnan, A., Dale, J.D., Brown, M.S. and Goldstein, J.L. (2008) Purified NPC1 protein. I. Binding of cholesterol and oxysterols to a 1278-amino acid membrane protein. *J. Biol. Chem.*, **283**, 1052–1063.

14. Ohgami, N., Ko, D.C., Thomas, M., Scott, M.P., Chang, C.C. and Chang, T.Y. (2004) Binding between the Niemann-Pick C1 protein and a photoactivatable cholesterol analog requires a functional sterol-sensing domain. *Proc. Natl Acad. Sci. USA*, **101**, 12473–12478.

15. Storch, J. and Xu, Z. (2009) Niemann-Pick C2 (NPC2) and intracellular cholesterol trafficking. *Biochim. Biophys. Acta*, **1791**, 671–678.

16. Infante, R.E., Wang, M.L., Radhakrishnan, A., Kwon, H.J., Brown, M.S. and Goldstein, J.L. (2008) NPC2 facilitates bidirectional transfer of cholesterol between NPC1 and lipid bilayers, a step in cholesterol egress from lysosomes. *Proc. Natl Acad. Sci. USA*, **105**, 15287–15292.

17. Cheruku, S.R., Xu, Z., Dutia, R., Lobel, P. and Storch, J. (2006) Mechanism of cholesterol transfer from the Niemann-Pick type C2 protein to model membranes supports a role in lysosomal cholesterol transport. *J. Biol. Chem.*, **281**, 31594–31604.

18. Ko, D.C., Gordon, M.D., Jin, J.Y. and Scott, M.P. (2001) Dynamic movements of organelles containing Niemann-Pick C1 protein: NPC1 involvement in late endocytic events. *Mol. Biol. Cell*, **12**, 601–614.

19. Blom, T.S., Linder, M.D., Snow, K., Pihko, H., Hess, M.W., Jokitalo, E., Veckman, V., Syvanen, A.C. and Ikonen, E. (2003) Defective endocytic trafficking of NPC1 and NPC2 underlying infantile Niemann-Pick type C disease. *Hum. Mol. Genet.*, **12**, 257–272.

20. Fessler, M.B. and Parks, J.S. (2011) Intracellular lipid flux and membrane microdomains as organizing principles in inflammatory cell signaling. *J. Immunol.*, **187**, 1529–1535.

21. Lloyd-Evans, E., Morgan, A.J., He, X., Smith, D.A., Elliot-Smith, E., Sillence, D.J., Churchill, G.C., Schuchman, E.H., Galione, A. and Platt, F.M. (2008) Niemann-Pick disease type C1 is a sphingosine storage disease that causes deregulation of lysosomal calcium. *Nat. Med.*, **14**, 1247–1255.

22. Zhang, J.R., Coleman, T., Langmade, S.J., Scherrer, D.E., Lane, L., Lanier, M.H., Feng, C., Sands, M.S., Schaffer, J.E., Semenkovich, C.F. *et al.* (2008) Niemann-Pick C1 protects against atherosclerosis in mice via regulation of macrophage intracellular cholesterol trafficking. *J. Clin. Invest.*, **118**, 2281–2290.

23. te Vruchte, D., Jeans, A., Platt, F.M. and Sillence, D.J. (2010) Glycosphingolipid storage leads to the enhanced degradation of the B cell receptor in Sandhoff disease mice. *J. Inherit. Metab. Dis.*, **33**, 261–270.

24. Loftus, S.K., Morris, J.A., Carstea, E.D., Gu, J.Z., Cummings, C., Brown, A., Ellison, J., Ohno, K., Rosenfeld, M.A., Tagle, D.A. *et al.* (1997) Murine model of Niemann-Pick C disease: mutation in a cholesterol homeostasis gene. *Science*, **277**, 232–235.

25. Somers, K.L., Wenger, D.A., Royals, M.A., Carstea, E.D., Connally, H.E., Kelly, T., Kimball, R. and Thrall, M.A. (1999) Complementation studies in human and feline Niemann-Pick type C disease. *Mol. Genet. Metab.*, **66**, 117–121.

26. Miyazaki, D., Nakamura, T., Toda, M., Cheung-Chau, K.W., Richardson, R.M. and Ono, S.J. (2005) Macrophage inflammatory protein-1alpha as a costimulatory signal for mast cell-mediated immediate hypersensitivity reactions. *J. Clin. Invest.*, **115**, 434–442.

27. Liu, B., Ramirez, C.M., Miller, A.M., Repa, J.J., Turley, S.D. and Dietschy, J.M. (2010) Cyclodextrin overcomes the transport defect in nearly every organ of NPC1 mice leading to excretion of sequestered cholesterol as bile acid. *J. Lipid Res.*, **51**, 933–944.

28. van Breemen, M.J., de Fost, M., Voerman, J.S., Laman, J.D., Boot, R.G., Maas, M., Hollak, C.E., Aerts, J.M. and Rezaee, F. (2007) Increased plasma macrophage inflammatory protein (MIP)-1alpha and MIP-1beta levels in type 1 Gaucher disease. *Biochim. Biophys. Acta*, **1772**, 788–796.

29. Sano, R., Tessitore, A., Ingrassia, A. and d'Azzo, A. (2005) Chemokine-induced recruitment of genetically modified bone marrow cells into the CNS of GM1-gangliosidosis mice corrects neuronal pathology. *Blood*, **106**, 2259–2268.

30. Ohmi, K., Greenberg, D.S., Rajavel, K.S., Ryazantsev, S., Li, H.H. and Neufeld, E.F. (2003) Activated microglia in cortex of mouse models of mucopolysaccharidoses I and IIIB. *Proc. Natl Acad. Sci. USA*, **100**, 1902–1907.

31. Wu, Y.P. and Proia, R.L. (2004) Deletion of macrophage-inflammatory protein 1 alpha retards neurodegeneration in Sandhoff disease mice. *Proc. Natl Acad. Sci. USA*, **101**, 8425–8430.

32. Dhami, R., Passini, M.A. and Schuchman, E.H. (2006) Identification of novel biomarkers for Niemann-Pick disease using gene expression analysis of acid sphingomyelinase knockout mice. *Mol. Ther.*, **13**, 556–564.

33. Gadola, S.D., Silk, J.D., Jeans, A., Illarionov, P.A., Salio, M., Besra, G.S., Dwek, R., Butters, T.D., Platt, F.M. and Cerundolo, V. (2006) Impaired selection of invariant natural killer T cells in diverse mouse models of glycosphingolipid lysosomal storage diseases. *J. Exp. Med.*, **203**, 2293–2303.

34. Ramirez, C.M., Liu, B., Taylor, A.M., Repa, J.J., Burns, D.K., Weinberg, A.G., Turley, S.D. and Dietschy, J.M. (2010) Weekly cyclodextrin administration normalizes cholesterol metabolism in nearly every organ of the Niemann-Pick type C1 mouse and markedly prolongs life. *Pediatr. Res.*, **68**, 309–315.

35. Lopez, M.E., Klein, A.D., Dimbil, U.J. and Scott, M.P. (2011) Anatomically defined neuron-based rescue of neurodegenerative Niemann-Pick type C disorder. *J. Neurosci.*, **31**, 4367–4378.

36. Tusher, V.G., Tibshirani, R. and Chu, G. (2001) Significance analysis of microarrays applied to the ionizing radiation response. *Proc. Natl Acad. Sci. USA*, **98**, 5116–5121.

37. Wada, R., Tifft, C.J. and Proia, R.L. (2000) Microglial activation precedes acute neurodegeneration in Sandhoff disease and is suppressed by bone marrow transplantation. *Proc. Natl Acad. Sci. USA*, **97**, 10954–10959.

38. Xu, Y.H., Jia, L., Quinn, B., Zamzow, M., Stringer, K., Aronow, B., Sun, Y., Zhang, W., Setchell, K.D. and Grabowski, G.A. (2011) Global gene expression profile progression in Gaucher disease mouse models. *BMC Genomics*, **12**, 20.

39. Tuppo, E.E. and Arias, H.R. (2005) The role of inflammation in Alzheimer's disease. *Int. J. Biochem. Cell Biol.*, **37**, 289–305.

40. Ray, A. and Dittel, B.N. (2010) Isolation of mouse peritoneal cavity cells. *J. Vis. Exp.*, **35**, e1488.

41. Gordon, S. and Taylor, P.R. (2005) Monocyte and macrophage heterogeneity. *Nat. Rev. Immunol.*, **5**, 953–964.

42. Fang, K.M., Wang, Y.L., Huang, M.C., Sun, S.H., Cheng, H. and Tzeng, S.F. (2011) Expression of macrophage inflammatory protein-1alpha and monocyte chemoattractant protein-1 in glioma-infiltrating microglia: involvement of ATP and P2X receptor. *J. Neurosci. Res.*, **89**, 199–211.

43. Cook, D.N., Beck, M.A., Coffman, T.M., Kirby, S.L., Sheridan, J.F., Pragnell, I.B. and Smithies, O. (1995) Requirement of MIP-1 alpha for an inflammatory response to viral infection. *Science*, **269**, 1583–1585.

44. Liu, B., Li, H., Repa, J.J., Turley, S.D. and Dietschy, J.M. (2008) Genetic variations and treatments that affect the lifespan of the NPC1 mouse. *J. Lipid Res.*, **49**, 663–669.

45. Parra, J., Klein, A.D., Castro, J., Morales, M.G., Mosqueira, M., Valencia, I., Cortes, V., Rigotti, A. and Zanlungo, S. (2011) Npc1 deficiency in the

C57BL/6J genetic background enhances Niemann-Pick disease type C spleen pathology. *Biochem. Biophys. Res. Commun.*, **413**, 400–406.

46. Faustino, J.V., Wang, X., Johnson, C.E., Klibanov, A., Derugin, N., Wendland, M.F. and Vexler, Z.S. (2011) Microglial cells contribute to endogenous brain defenses after acute neonatal focal stroke. *J. Neurosci.*, **31**, 12992–13001.

47. Buiting, A.M. and Van Rooijen, N. (1994) Liposome mediated depletion of macrophages: an approach for fundamental studies. *J. Drug Target*, **2**, 357–362.

48. Rong, Y., Wang, T. and Morgan, J.I. (2004) Identification of candidate Purkinje cell-specific markers by gene expression profiling in wild-type and pcd(3J) mice. *Mol. Brain Res.*, **132**, 128–145.

49. Sarna, J.R., Larouche, M., Marzban, H., Sillitoe, R.V., Rancourt, D.E. and Hawkes, R. (2003) Patterned Purkinje cell degeneration in mouse models of Niemann-Pick type C disease. *J. Comp. Neurol.*, **456**, 279–291.

50. Perry, V.H. and O'Connor, V. (2008) C1q: the perfect complement for a synaptic feast? *Nat. Rev. Neurosci.*, **9**, 807–811.

51. Yu, T., Shakkottai, V.G., Chung, C. and Lieberman, A.P. (2011) Temporal and cell-specific deletion establishes that neuronal Npc1 deficiency is sufficient to mediate neurodegeneration. *Hum. Mol. Genet.*, **20**, 4440–4451.

52. Zu, T., Duvick, L.A., Kaytor, M.D., Berlinger, M.S., Zoghbi, H.Y., Clark, H.B. and Orr, H.T. (2004) Recovery from polyglutamine-induced neurodegeneration in conditional SCA1 transgenic mice. *J. Neurosci.*, **24**, 8853–8861.

53. Ko, D.C., Milenkovic, L., Beier, S.M., Manuel, H., Buchanan, J. and Scott, M.P. (2005) Cell-autonomous death of cerebellar purkinje neurons with autophagy in Niemann-Pick type C disease. *PLoS Genet.*, **1**, 81–95.

54. Beltroy, E.P., Liu, B., Dietschy, J.M. and Turley, S.D. (2007) Lysosomal unesterified cholesterol content correlates with liver cell death in murine Niemann-Pick type C disease. *J. Lipid. Res.*, **48**, 869–881.

55. Palmeri, S., Tarugi, P., Sicurelli, F., Buccoliero, R., Malandrini, A., De Santi, M.M., Marciano, G., Battisti, C., Dotti, M.T., Calandra, S. *et al.* (2005) Lung involvement in Niemann-Pick disease type C1: improvement with bronchoalveolar lavage. *Neurol. Sci.*, **26**, 171–173.

56. Yerushalmi, B., Sokol, R.J., Narkewicz, M.R., Smith, D., Ashmead, J.W. and Wenger, D.A. (2002) Niemann-pick disease type C in neonatal cholestasis at a North American Center. *J. Pediatr. Gastroenterol. Nutr.*, **35**, 44–50.

57. Hochedlinger, K., Yamada, Y., Beard, C. and Jaenisch, R. (2005) Ectopic expression of Oct-4 blocks progenitor-cell differentiation and causes dysplasia in epithelial tissues. *Cell*, **121**, 465–477.

58. Rimkunas, V.M., Graham, M.J., Crooke, R.M. and Liscum, L. (2009) TNF-{alpha} plays a role in hepatocyte apoptosis in Niemann-Pick type C liver disease. *J. Lipid Res.*, **50**, 327–333.

59. Serhan, C.N. and Savill, J. (2005) Resolution of inflammation: the beginning programs the end. *Nat. Immunol.*, **6**, 1191–1197.

60. Peake, K.B., Campenot, R.B., Vance, D.E. and Vance, J.E. (2011) Niemann-Pick Type C1 deficiency in microglia does not cause neuron death in vitro. *Biochim. Biophys. Acta*, **1812**, 1121–1129.

61. Elrick, M.J., Pacheco, C.D., Yu, T., Dadgar, N., Shakkottai, V.G., Ware, C., Paulson, H.L. and Lieberman, A.P. (2010) Conditional Niemann-Pick C mice demonstrate cell autonomous Purkinje cell neurodegeneration. *Hum. Mol. Genet.*, **19**, 837–847.

62. Finkelstein, A., Kunis, G., Seksenyan, A., Ronen, A., Berkutzki, T., Azoulay, D., Koronyo-Hamaoui, M. and Schwartz, M. (2011) Abnormal changes in NKT cells, the IGF-1 axis, and liver pathology in an animal model of ALS. *PLoS ONE*, **6**, e22374.

63. Patterson, M.C. (2003) A riddle wrapped in a mystery: understanding Niemann-Pick disease, type C. *Neurologist*, **9**, 301–310.

64. Zhang, J. and Erickson, R.P. (2000) A modifier of Niemann Pick C 1 maps to mouse chromosome 19. *Mamm. Genome*, **11**, 69–71.

65. Carette, J.E., Raaben, M., Wong, A.C., Herbert, A.S., Obernosterer, G., Mulherkar, N., Kuehne, A.I., Kranzusch, P.J., Griffin, A.M., Ruthel, G. *et al.* (2011) Ebola virus entry requires the cholesterol transporter Niemann-Pick C1. *Nature*, **477**, 340–343.

66. Edgar, R., Domrachev, M. and Lash, A.E. (2002) Gene Expression Omnibus: NCBI gene expression and hybridization array data repository. *Nucleic Acids Res.*, **30**, 207–210.

67. Huang Da, W., Sherman, B.T. and Lempicki, R.A. (2009) Systematic and integrative analysis of large gene lists using DAVID bioinformatics resources. *Nat. Protoc.*, **4**, 44–57.